A Hybrid Approach for Microscopic Properties and Self-Assembly of Dendrimers between Two Hard Walls

Lisheng Cheng and Dapeng Cao*

Division of Molecular and Materials Simulation, Key Lab of Nanomaterials, Ministry of Education Beijing University of Chemical Technology, Beijing 100029, People's Republic of China

Received: April 3, 2007; In Final Form: June 25, 2007

Dendrimers are of interest in a number of applications and theoretical studies due to their interesting and complex architectures. We use a hybrid approach to investigate the microstructure of hard dendrimers and self-assembly of diblock dendrimers confined between two hard walls. In the hybrid approach, a single-chain Monte Carlo simulation is used to evaluate the ideal-gas contribution of the Helmholtz energy and a density functional theory is employed to calculate the excess Helmholtz energy. In our calculations, a coarse-grained model is used to represent the dendrimers of generations 1−4. The effects of generation and bulk packing fraction on the microscopic properties of the hard dendrimers are explored. With the increase of generations, the complexity of the dendritic architecture increases. Accordingly, the depletion effect becomes stronger with the generation at $\eta_{bulk} = 0.1$. Furthermore, it is found that the more complex the molecular architecture and the higher the molecular stiffness, the smaller is the partitioning coefficient of confined dendrimers. In addition, we also investigate the effects of the width of the slit and the interaction (ϵ^*_{AA}) between hydrophilic segments on the self-assembly of diblock dendrimers in the slit. With the increase of ϵ^*_{AA}, we observe that the curves of average packing fraction of the dendrimers in the slit exist an abrupt jump, which corresponds to the first-order phase transition from a disordered state to a lamellar ordered structure. In the slit of $H = 11\sigma$, it is at $\epsilon^*_{AA} = 8$ rather than $\epsilon^*_{AA} = 10$ or $\epsilon^*_{AA} = 12$ that the minimum critical bulk packing fraction appears. This observation is distinctively different from the case of self-assembly of rod-like molecules in the slit, where the critical bulk concentration increases with the decrease of the head−head interaction linearly.

1. Introduction

Dendritic architecture is one of the most pervasive but interesting topologies in nature at the scales of meso- and microscopic levels and has been recognized as a fourth major new class of macromolecular architectures.[1−3] Development of the extensive synthetic methods, such as divergent and convergent hierarchical strategies, leads to experimental preparation of various dendritic structures. Currently, these polymers with dendritic architectures consist of four subclasses: (1) random hyperbranched polymers, (2) dendrigraft polymers, (3) dendrons, and (4) dendrimers. The schematic diagrams of the four dendritic architectures can be referred to in literature.[4] The order of this subclass from (1) to (4) reflects the relative degree of structural control in these dendritic architectures.[1,5] Obviously, the random hyperbranched polymers have random dendritic architectures while the dendrimers possess highly hierarchical ordered architectures. The dendrimer consists of a core shell structure, which is characterized by a central core, interior shells (generation) consisting of repeating branch-cell units, and terminal functional groups (the outer shell or periphery).[4]

The first poly(amidoamine) (PAMAM) dendrimer was synthesized by Tomalia in 1985, and the term "dendrimer" was formally coined by Tomalia.[6] In fact, the first dendrimer was prepared in 1978.[7] However, it was named a "cascade molecule" at that time.[8] Due to their unique structure-controlled properties during synthesis, dendrimers are the most interesting one among dendritic polymers and have a variety of technological applications, such as drug delivery devices,[9−12] catalytic devices,[13−15] photochemical devices,[16−18] electrochemical devices,[19,20] and separations.[21−23]

In the past decades, many efforts have been made to predict microstructures and physicochemical properties of dendrimers in aqueous solutions[24−26] and near the surface.[27] Han et al.[24] used a molecular dynamics simulation to calculate the properties of ethylenediamine (EDA) cored PAMAM dendrimers of generations 1−7 in an aqueous solution and found that the dendrimers of all generations are spherical in shape; the higher generations show edges or are slightly polyhedral in shape, while the EDA core of the dendrimer deviated from the center of the sphere, especially for those with the lower generations. Mansfield[27] found that with the increase of interaction between the dendrimer and surface, the dendrimer was observed to spread out and flatten down on the surface. Gorman et al.[28] found that flexible-unit dendrimers were globular but not completely spherical, while stiff-unit dendrimers had a more eccentric disk-like shape. Welch[29] used a Brownian dynamics simulation to design a dendrimer−polymer conjugate containing a dendritic and a linear block as a tunable molecular actuator. They found the device could be tuned by the strength of an external electric field. Subsequently, Zhou and Chen[30] also simulated conformational properties of a neutral dendrimer−polymer conjugate using off-lattice Monte Carlo method. Suek and Lamm[25] used a molecular dynamics method to explore the effect of terminal group modification on solution properties of dendrimers. Recently, the phase behavior of model dendrimers of generations

* To whom correspondence should be addressed. E-mail: caodp@mail.buct.edu.cn or cao_dp@hotmail.com.

10.1021/jp072631m CCC: $37.00
Published on Web 08/18/2007

2−5 was simulated on the basis of the lattice model.[31] Interestingly, the above calculations and predictions are from molecular simulations including molecular dynamics and Monte Carlo simulations.[32] With the development of statistical mechanics and free-energy functional theory, the density functional theory (DFT) provides an alternative to predict the physical properties of polymers.

Since Chandler, McCoy, and Singer[33] proposed the DFT, which can be applicable to bulk and inhomogeneous polymeric systems,[34−36] many other versions of the DFT have been developed, such as Kierlik and Rosinberg (KR),[37] Yu and Wu (YW),[38] White-Bear,[39] Tripathi and Chapman (TC),[40] and Ye et al. (YCLH)[41]. Among them, the modified fundamental measure theory (MFMT)-based DFT has been extensively applied to investigate microstructures and thermodynamics properties of linear,[42−45] multivalent,[46] hard disk,[47] semi-flexible and rod-like,[48−50] and star polymers.[51] In addition, the MFMT-based DFT was also used to calculate adsorption and phase transition of model polymers[52−56] and the solvation force between polymer brushes.[57] All these investigations indicate that the MFMT-based DFT is not only highly suitable for the polymeric fluids but also very accurate in numerical calculations compared to simulation data. In these investigations, the molecular architectures are basically restricted in simple models like flexible and rigid linear chains. Due to the architecture complexity of the dendrimers, integration of chain connectivity in the MFMT-based DFT becomes extremely difficult and almost cannot be solved analytically, especially for the dendrimers of high generations. Although a lot of computer simulations have been applied to explore properties of dendrimers under different conditions,[24,26,31,58] no reports from DFT are available for the dendrimers.

As a result, we use a hybrid approach to study microstructures and thermodynamic properties of dendrimers confined between two hard walls. The hybrid approach contains a single-chain simulation for the evaluation of the ideal part of the Helmholtz energy and an MFMT-based DFT for the calculation of excess Helmholtz energy. The hybrid approach avoids the complex integral of dendrimer chain connectivity by calculating the statistical average of single molecular chains. Simultaneously, the hybrid approach also contains the volume-exclude effect from MFMT. To our knowledge, it is the first report on the use of DFT to investigate microscopic properties of confined dendrimers.

The rest of this paper is organized as below. First, we depict the models of the dendrimer and the hybrid approach in detail. Second, we investigate the effects of generations and bulk packing fraction on microstructures of the confined dendrimers in athermal systems. Third, the self-assembly of the confined dendrimers in thermal systems is explored. Finally, some discussion is addressed.

2. Theory and Molecular Models

2.1. Molecular Models. A coarse-grained model is used to represent the hard dendrimers, where the bonding length between two segments is fixed as the segmental diameter and the bonding angle is fully flexible. As mentioned in the Introduction, the dendrimer molecule is a core−shell architecture. The number of segments tangentially connected to the core is defined as the arm of the dendrimer. All segments tangentially connected to the core are defined as generation 1 of the shell architecture, and those connected to the segments of generation 1 are defined as generation 2. The rest may be deduced by analogy. In this work, the number of the arm is fixed at 3 and

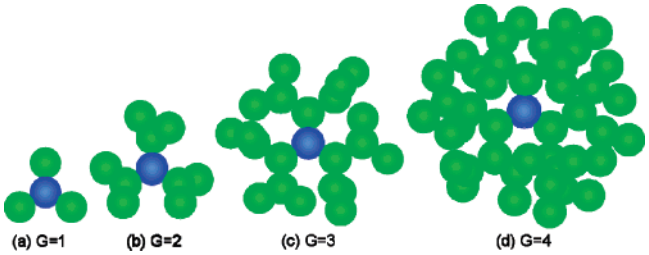

Figure 1. Hard dendrimer models of generation 1−4, where the "O" segment is blue and the "B" segments are green.

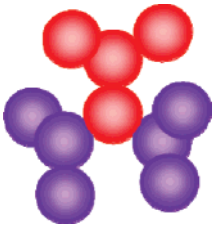

Figure 2. Diblock dendrimer model of generation 2, where "A" segments are red and "B" segments are purple.

generations of the dendrimer change from 1−4. The schematic diagrams of the dendrimers of generations 1−4 are shown in Figure 1a−d, respectively.

To efficiently generate the configurations of dendrimers for the single-chain simulation, the number of segments of the dendrimer molecule of generation G can be calculated by

$$M = Q \times (2^{G} - 1) + 1 \tag{1}$$

where Q is the number of arms and is equal to 3 in this work. In particular, the number of segments in the shell of generation n is $M' = Q \times 2^{n-1}$. Here, we consider an athermal system and a thermal system. In the athermal system, to distinguish the core of the dendrimer, we define the "core" segment as "O" and the other segments as "B" and use the hard-sphere potential to represent the interactions between segments and between the hard wall and segments.

In the thermal systems, the diblock dendrimer contains two types of segments with different properties. The two types of segments are denoted as "A" and "B". The former represents the hydrophilic segments, and the latter represents the hydrophobic segments. The schematic diagram of the diblock dendrimer of generation 2 is shown in Figure 2. The interaction between the segments and hard walls is also described by the hard-sphere potential, but the pair interactions between these segments are represented by short-ranged attractive square-well (SW) potential expressed as

$$\varphi_{ij}(r) = \begin{cases} \infty, & r < \sigma \\ \epsilon_{i,j}, & \sigma \le r \le \gamma\sigma \\ 0, & r \ge \sigma \end{cases} \tag{2}$$

where σ is the segmental diameter and r is the distance between two segments.

2.2. Density Functional Theory. The Helmholtz energy functional $F[\rho_M(\mathbf{R})]$ is conventionally expressed as an ideal contribution corresponding to the system of ideal chains that interact only through bonding potentials and an excess contribution that takes into account the interactions of nonbonded chain connectivity, hard-sphere repulsion, and van der Waals attraction, given by[42]

$$F[\rho_M(\mathbf{R})] = F_{id}[\rho_M(\mathbf{R})] + \boldsymbol{F}_{ex}[\rho(\mathbf{r})] \tag{3}$$

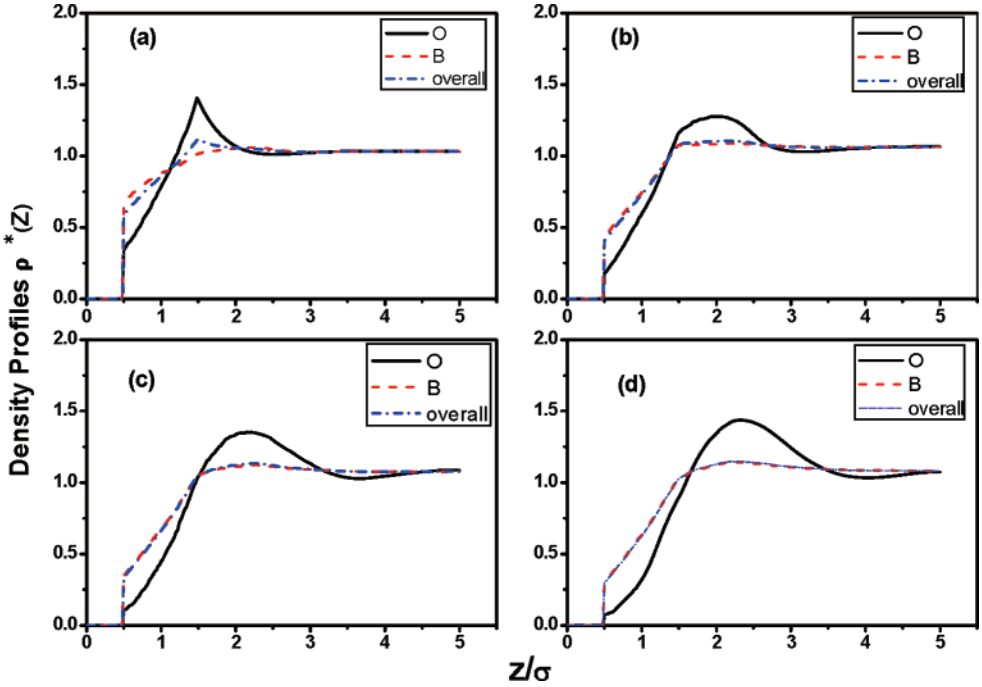

Figure 3. Segmental density profiles of the dendrimers confined between two hard walls separated by pore width $H = 10\sigma$ at bulk packing fraction $\eta = 0.10$: (a) generation 1; (b) generation 2; (c) generation 3; (d) generation 4.The density profiles are normalized to the average density in the slit.

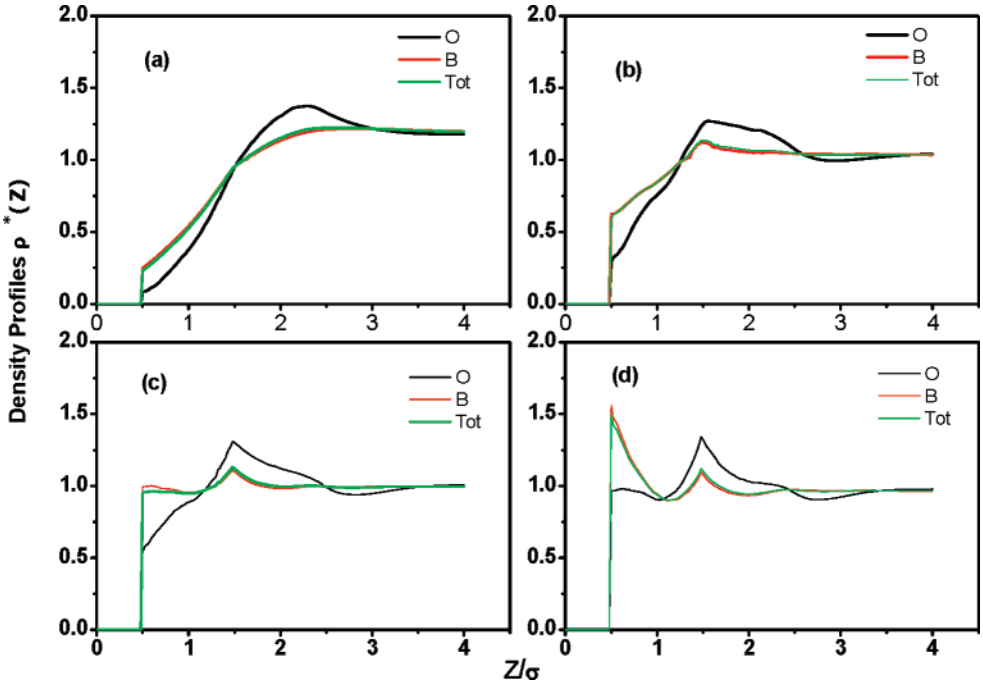

Figure 4. Segmental density profiles of the dendrimer of G2 confined between two hard walls separated by pore width $H = 8\sigma$ at bulk volume fraction: (a) $\eta_{bulk} = 0.04$; (b) $\eta_{bulk} = 0.14$; (c) $\eta_{bulk} = 0.20$; (d) $\eta_{bulk} = 0.26$.

where $\rho_M(\mathbf{R})$ is a multidimensional density profile and $\mathbf{R}$ is a composite vector $(\mathbf{r}_1,\mathbf{r}_2, ..., \mathbf{r}_M)$ representing the positions of all segments of a dendrimer. The subscript M indicates the number of segments of the molecule. The molecular density profile $\rho_M(\mathbf{R})$ is related to the segmental densities by

$$\rho(\mathbf{r}) = \sum_{i=1}^{M} \rho_{si}(\mathbf{r}) = \sum_{i=1}^{M} \int d\mathbf{R}\, \delta(\mathbf{r} - \mathbf{r}_i)\rho_M(\mathbf{R}) \qquad (4)$$

where $\rho(\mathbf{r})$ is the total segmental density, $\rho_{si}(\mathbf{r})$ is the local density of segment i, and $d\mathbf{R}$ stands for a set of differential volumes $(d\mathbf{r}_1, d\mathbf{r}_2, ..., d\mathbf{r}_M)$.

For the ideal polymer system with only bonding potentials, the Helmholtz energy is known exactly as

$$\beta F_{id}[\rho_M(\mathbf{R})] = \int d\mathbf{R}\rho_M(\mathbf{R})[\ln \rho_M(\mathbf{R}) - 1] + \beta \int d\mathbf{R}\rho_M(\mathbf{R})V_B(\mathbf{R}) \quad (5)$$

where the $V_B(\mathbf{R})$ is the direct bond potential $\beta = (kT)^{-1}$, with k being Boltzmann constant and T temperature.

The excess part of the Helmholtz energy functional can be mathematically expressed as a summation of contributions from

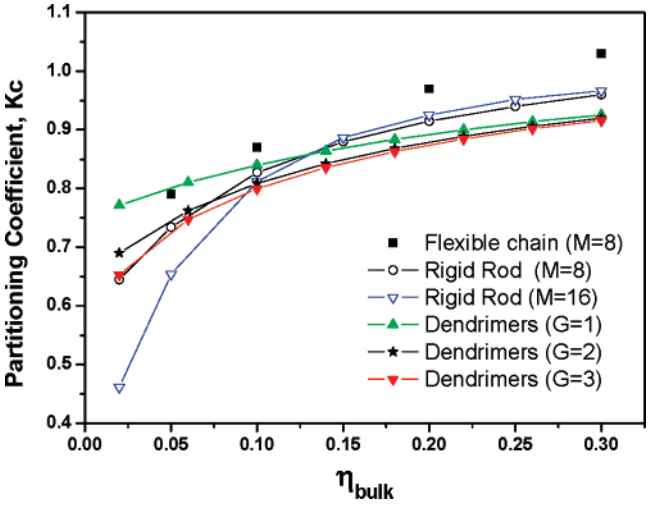

Figure 5. Partitioning coefficients of dendrimers with G1−G3 as a function of bulk packing fraction at pore width $H = 10\sigma$. Partitioning coefficients of rigid rods of $M = 8$ and 16 and flexible chains of $M = 8$ are also included in the figure for comparison.[49]

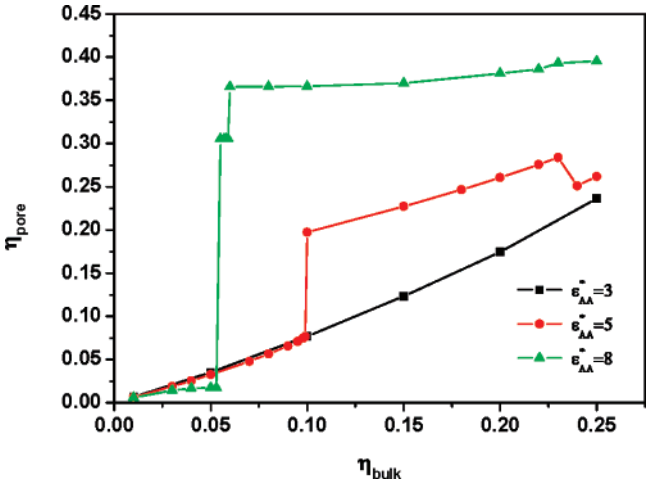

Figure 6. The average packing fractions of segments of the dendrimers in the slit of $H = 8\sigma$ as a function of bulk packing fraction at different ϵ^*_{AA}, where $\epsilon^*_{AB} = -1$ and $\epsilon^*_{BB} = 1$ (negative stands for the repulsion).

the hard-sphere repulsion, correlations due to chain connectivity, and van der Waals attractions, given by

$$\beta F_{ex}[\rho(\mathbf{r})] = \beta F_{ex}^{hs} + \beta F_{ex}^{chain} + \beta F_{ex}^{att} \quad (6)$$

Following our previous work for polymers,[42,48] the hard-sphere part (βF_{ex}^{hs}) of the Helmholtz energy functional is represented by a modified fundamental measure theory

$$\beta F_{hs} = \int d\mathbf{r} \left\{ -n_0 \ln(1-n_3) + \frac{n_1 n_2 - \mathbf{n}_{V1}\cdot\mathbf{n}_{V}2}{1-n_3} + (n_2{}^3/3 - n_2 \mathbf{n}_{V_2}\cdot\mathbf{n}_{V_2}) \left[\frac{\ln(1-n_3)}{12\pi n_3{}^2} + \frac{1}{12\pi n_3 (1-n_3)^2} \right] \right\} \quad (7)$$

where $n_\alpha(\mathbf{r})$ ($\alpha = 0, 1, 2, 3, V_1, V_2$) are scalar and vector weighted densities defined by Rosenfeld[59] as

$$n_\alpha(\mathbf{r}) = \sum_j n_{\alpha j}(\mathbf{r}) = \sum_j \int \rho_j(\mathbf{r}')\, \omega_j^\alpha(\mathbf{r}-\mathbf{r}')\, d\mathbf{r}' \quad (8)$$

and $\bar{\omega}_j^\alpha$ ($\alpha = 0, 1, 2, 3, V_1, V_2$) are weight functions. The excess Helmholtz energy functional due to the chain connectivity is given by a generalized first-order thermodynamics perturbation theory[46,48]

$$\beta F_{chain} = \int d\mathbf{r}\, \frac{1-M}{M}\, n_0 \cdot \xi \cdot \ln y^{hs}(\sigma, n_\alpha) \quad (9)$$

where $\xi = 1 - \mathbf{n}_{V_2}\cdot\mathbf{n}_{V_2}/n_2{}^2$, and $y^{hs}(\sigma,n_\alpha)$ is the contact value of the cavity correlation function for hard-sphere segments

$$y^{hs}(\sigma,n_\alpha) = \frac{1}{1-n_3} + \frac{n_2\xi\sigma}{4(1-n_3)^2} + \frac{n_2{}^2\xi\sigma}{72(1-n_3)^3} \quad (10)$$

The Helmholtz energy given by eq 9 is not directly related to the bonding potentials of polymeric molecules. Instead, this term takes into account the effect of chain connectivity on the correlations between polymeric segments.

The excess Helmholtz energy functional due to van der Waals attractions, βF_{ex}^{att}, is represented by a mean-field approximation[48]

$$\beta F_{ex}^{att} = \frac{1}{2} \int\int d\mathbf{r}\, d\mathbf{r}' \sum_{i,j=A,B} \rho_i(\mathbf{r})\, \rho_j(\mathbf{r}) \beta \varphi_{ij}^{att}(|\mathbf{r}-\mathbf{r}'|) \quad (11)$$

where $\varphi_{ij}^{att}(r)$ is the van der Waals potential between segments described in eq 2.

For a polymeric fluid, the grand potential is related to the Helmholtz energy functional $F[\rho_M(\mathbf{R})]$ via the Legendre transform

$$\Omega[\rho_M(\mathbf{R})] = F[\rho_M(\mathbf{R})] + \int [\psi_M(\mathbf{R}) - \mu_M]\rho_M(\mathbf{R})\, d\mathbf{R} \quad (12)$$

where $\psi_M(\mathbf{R})$ is the external potential exerting on individual segments and μ_M is the chemical potential of a polymer chain.[42] Minimization of the grand potential with respect to the density profiles, namely, eq 12, yields the Euler−Lagrange equation

$$\rho_M(\mathbf{R}) = \exp[\beta\mu_M - \beta V_B(\mathbf{R}) - \beta \sum_{i=1}^{M} \lambda_i(\mathbf{r}_i)] \quad (13)$$

where the self-consistent potential $\lambda_i(\mathbf{r}_i)$ includes the derivative of the excess Helmholtz free-energy and the external potential $\varphi_i(\mathbf{r}_i)$,

$$\lambda_i(\mathbf{r}_i) = \frac{\delta F_{ex}}{\delta \rho(\mathbf{r}_i)} + \varphi_i(\mathbf{r}_i) \quad (14)$$

Combination of eqs 4, 13, and 14 yields the segmental densities $\rho_{si}(\mathbf{r})$

$$\rho_{si}(\mathbf{r}) = \int d\mathbf{R}\, \delta(\mathbf{r}-\mathbf{r}_i) \exp[\beta\mu_M - \beta V_B(\mathbf{R}) - \beta \sum_{j=1}^{M} \lambda_j(\mathbf{r}_j)] \quad (15)$$

where $\exp[-\beta V_B(\mathbf{R})]$ represents the probability density of an ideal hard dendrimer with configuration $\mathbf{R}$.[48] For simplicity, let $P(\mathbf{R}) = \exp[-\beta V_B(\mathbf{R})]$. In the hybrid approach, the probability density $P(\mathbf{R})$ can be attained by carrying out single-chain simulations with sufficient conformations filling the whole configurational space rather than by the integral of the Dirac

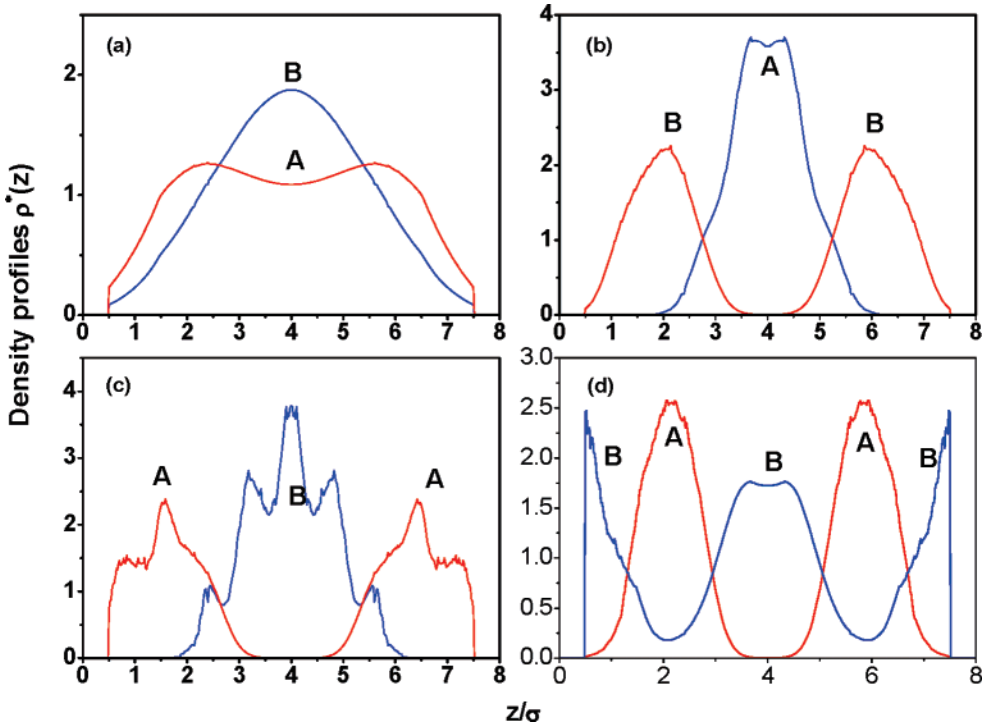

Figure 7. Microstructures of the dendrimers of G2 in the slit of $H = 8\sigma$ at $\epsilon^*_{AA} = 5$ and different bulk packing fraction: (a) $\eta_{bulk} = 0.099$; (b) $\eta_{bulk} = 0.1$; (c) $\eta_{bulk} = 0.234$; (d) $\eta_{bulk} = 0.235$.

delta functions used in the previous DFT approach.[51] Equation 15 can be reformulated as

$$\rho_{si}(\mathbf{r}) = \exp(\beta\mu_M) \int d\mathbf{R}\, \delta(\mathbf{r} - \mathbf{r}_i)\cdot P(\mathbf{R})\cdot \exp[-\beta \sum_{j=1}^{M} \lambda_j(\mathbf{r}_j)] \quad (16)$$

By the average of lots of configurations from the single-chain simulation,[50,60,61] we get

$$\rho_{si}(\mathbf{r}) = \exp(\beta\mu_M)\langle \exp[-\beta \sum_{j=1}^{M} \lambda_j(\mathbf{r}_j)]\rangle_{\mathbf{r}=\mathbf{r}_i} \quad (17)$$

where $\langle\rangle$ is the average of all configurations of the single molecules that are independent of the density profiles and the external fields. In particular, in the calculation of local density of segment i, $\rho_{si}(\mathbf{r})$, the segment i is put in the fixed position $\mathbf{r}$. Then, the positions (r_j) of the other segments of the given single dendrimer are known. As a result, the self-consistent potentials, $\lambda_j(r_j)$, related to all the positions (r_j, $j = 1, 2, ..., M$), can be used in eq 17 to obtain the ensemble average. To efficiently represent the whole configurational space, we use a large number ($\sim 10^5$) of dendrimer conformations to calculate the ensemble average of eq 17. Compared to the complex integral of the Dirac delta functions used in the pure DFT,[48,51] the hybrid method provides less computational cost and simpler expression, because the direct integral of application of pure DFT in a star polymer is fairly complex and has to bear the large time consumption for the recurrence functions.[51]

In our calculations, the Picard iterative method was used to solve eq 17.[49] The iteration started from the bulk density of the dendrimers. After a new density profile was obtained, we would combine the new density and the previous one in an appropriate prescription as a new input. Then, the self-consistent potential was modified by eq 14. Iterations were repeated until the deviation between the old density and the new one was smaller than the scheduled error at all the points. It should be pointed out that the hybrid approach has been tested and has been shown to have excellent performance in comparison to Monte Carlo data.[50,60,61]

3. Results and Discussion

3.1. Athermal Systems. The complex architecture of the dendrimer is closely related to generations, because the generations determine the number of the shell layers around the core in the dendrimer. First, we consider these systems of dendrimers containing different generations. Figure 3 shows microstructures of the dendrimers with the generations 1−4 (G1−G4) at packing fraction $\eta_{bulk} = 0.10$ and pore width $H = 10\sigma$, where σ is the diameter of the segment. For all generations of the dendrimer, the depletion effect is observed near the surface. The presence of the surface leads to the loss of configurational entropy of the dendrimer. As a result, the contact values of the local densities of the dendrimer are smaller than the bulk density at $\eta_{bulk} = 0.10$.

It can be observed from Figure 3 that the contact value of the "O" segment (i.e., the core) is always smaller than those of "B" segments for all the cases studied, which means that the core segment has less possibility than "B" segments to contact the hard wall. When the "O" segments contact the wall, the dendrimers would lose more configurational entropy. With the increase of the generations, the contact value of total density of the dendrimers apparently drops from 0.6 for G1 to 0.3 for G4. There are two reasons for the decrease of the contact value. First, at the fixed packing fraction of $\eta_{bulk} = 0.10$, the molecular density decreases with the increase of the generation. Second, the depletion effect becomes stronger with the increase of the generations because the complexity of the dendritic architecture increases with the generations.

Note that the dendrimer of G1 shows an abrupt peak in the local density profiles of the core segment "O", while the dendrimers of G2−G4 present smooth peaks in the local density

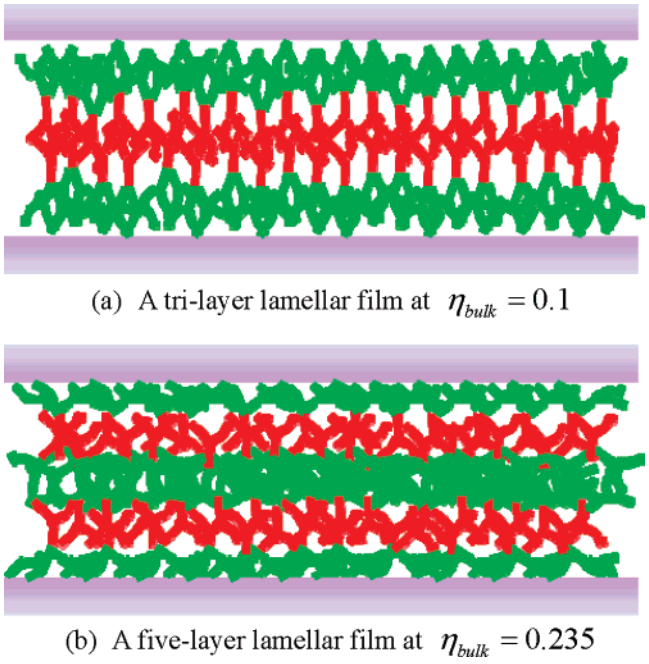

Figure 8. Schematic diagrams for two lamellar thin films formed by the self-assembly of dendrimers in the silt of $H = 8\sigma$ at $\epsilon^*_{AB} = 5$: (a) a trilayer lamellar film at $\eta_{bulk} = 0.1$; (b) a five-layer lamellar film at $\eta_{bulk} = 0.235$.

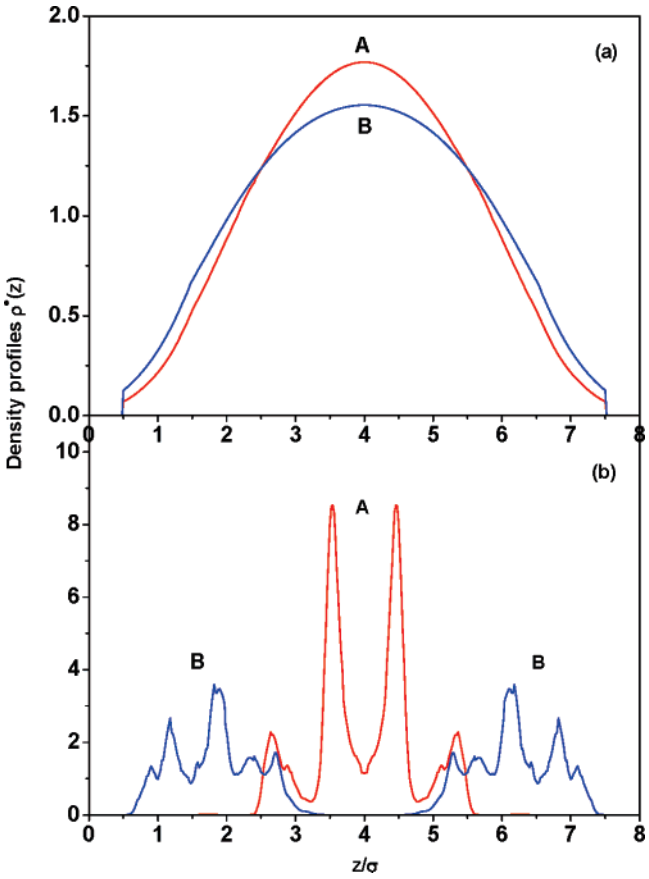

Figure 9. Microstructure of the dendrimers of G2 in the slit of $H = 8\sigma$ at $\epsilon^*_{AA} = 8$ and different bulk packing fractions: (a) $\eta_{bulk} = 0.054$; (b) $\eta_{bulk} = 0.055$.

profiles of the core segment "O". Furthermore, the position of the peak increases from $z = 1.5\sigma$ for G1 to $z = 2.5\sigma$ for G4. On the contrary, the total densities of the dendrimers do not present any distinguishable peaks, which is similar with that of a hard sphere. The observation is the same as that reported by Han et al.,[24] where they found that the dendrimers show the behavior of spherical molecules.

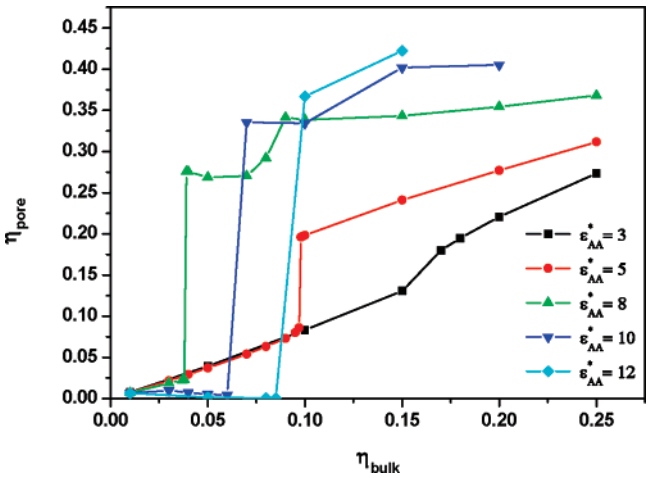

Figure 10. Average packing fraction of segments of the dendrimers in the slit of $H = 11\sigma$ as a function of bulk packing fraction at different ϵ^*_{AA}, where $\epsilon^*_{AB} = -1$, and $\epsilon^*_{BB} = 1$ (negative stands for the repulsion).

In order to get insight into the effect of bulk packing fraction on the microstructure of the dendrimer, we present in Figure 4 the local density profiles of dendrimers of G2 at different bulk packing fractions, $\eta = 0.04$, 0.14, 0.2, and 0.26. It can be found that a strong depletion effect appears at low bulk packing fraction $\eta = 0.04$, and the contact value of the total density of the dendrimer is equal to 0.3, which is smaller than the bulk density. With the increase of the bulk packing fraction, the contact value of total density of the dendrimer increases and reaches 1.6 at $\eta = 0.26$. As is well-known, there exists a competition for the confined fluids between the depletion effect and the packing effect. In general, the depletion effect dominates the competition at low bulk packing fractions while the packing effect does at high bulk packing fractions. Therefore, the packing effect would replace the depletion effect with the increase of the bulk packing fraction. In this case, the packing effect was observed only at $\eta = 0.26$, while the packing effect can be observed at $\eta = 0.2$ for linear chains with the same chain length. Hence, the structural complexity of the dendrimer leads to the increase of critical bulk packing fraction corresponding to the transition from the depletion effect to the packing effect. In addition, due to the more restriction of the core segment "O", the contact value of the core segment "O" is always smaller than that of the segment "B". Impressively, at $\eta = 0.26$, the total density of the dendrimer presents a bilayer structure including a contact layer and second layer. Note that the local density of the core segment "O" is not overlapping with the total density of the dendrimer for all cases, which is the same as in Figure 3.

In investigations of confined fluids, the partitioning coefficient is often used to explore the difference between packing fractions in bulk and confined phases. So, we also considered the partitioning coefficient of dendrimers, which is defined as the packing fraction in the confined phase divided by the one in bulk phase, given by

$$K_c = \rho^{ave}_{pore}/\rho_{bulk} = \eta_{pore}/\eta_{bulk}$$

Figure 5 shows the partitioning coefficients of dendrimers of generations 1−3 as a function of packing fraction in the bulk phase. For comparison, the partitioning coefficient of the flexible

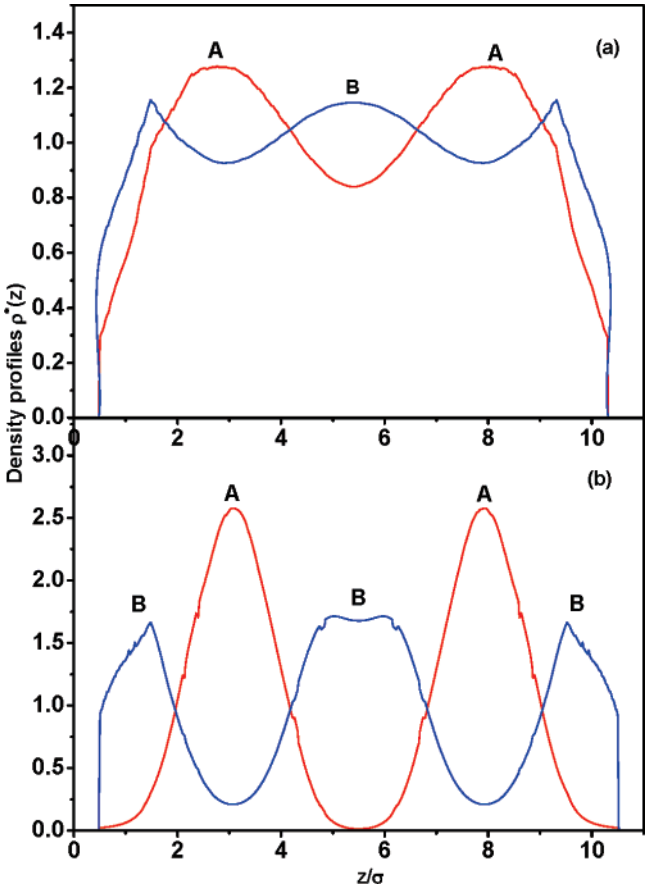

Figure 11. Microstructures of the dendrimers of G2 in the slit of $H = 11\sigma$ at $\epsilon^*_{AA} = 3$ and different bulk packing fractions: (a) $\eta_{bulk} = 0.15$; (b) $\eta_{bulk} = 0.17$.

chain of $M = 8$ and those of the rod polymers[49] of $M = 8$ and 16 were also inserted into Figure 5. For the dendrimer of interest, all the partitioning coefficients are smaller than 1.0. It means that the packing fraction of dendrimers in the confined phase is less than that in the bulk phase because the hard dendrimers do not like to enter into the confinement due to the presence of two hard surfaces. In addition, it is found that the partitioning coefficient of the dendrimers of G3 is the smallest among the three dendrimers studied. It suggests that the dendrimer of G3 is more difficult to enter the confinement than that of G1 because the dendrimer of G3 holds a more complex architecture. Obviously, the linear, flexible chain of $M = 8$ provides the largest partitioning coefficient in Figure 5 because the flexible chain would lose less configurational entropy upon entering the confinement. Interestingly, at low bulk packing fractions, $\eta_{bulk} < 0.1$, it is the rod-like molecule of $M = 16$ rather than the dendrimer molecule that provides the smallest partitioning coefficient. Hence, in this case, the rod-like molecule of $M = 16$ would lose more configurational entropy. To enter the confinement of $H = 10\sigma$, the rod-like molecule of $M = 16$ has to adjust their orientations parallel to the surface, which leads to the loss of more configurational entropy. As a result, the partitioning coefficient is closely related not only to the molecular architecture but also to the molecular stiffness. The more complex the molecular architecture and higher the molecular stiffness, the smaller is partitioning coefficient.

3.2. Thermal Systems. In the above section, we have investigated the microscopic behavior of hard dendrimers between two hard walls in an athermal system. However, we believe that it is more interesting to investigate the behavior of a diblock dendrimer in a thermal system because the diblock dendrimer contains two types of segments with different properties. Therefore, in this section we explore the self-assembly behavior of diblock dendrimers between two hard walls in a thermal system. In this calculation, we consider the diblock dendrimer of G2, where the diblcok dendrimer includes one hydrophilic arm composed of "A" segments and two hydrophobic arms composed of "B" segments. The schematic diagram is shown in Figure 2. To gain insight into self-assembly of the diblock dendrimers between two hard walls, we employ the SW potential in eq 2 to represent the short-ranged attraction between the like segments. To enhance the microscopic phase separation of "A" and "B" blocks, we use a slightly repulsive SW potential to represent the interaction between the unlike segments (i.e., the interaction between "A" and "B" segments). In this work, $\epsilon^*_{BB} = 1$ and $\epsilon^*_{AB} = -1$ (negative indicates the repulsion). To explore the effect of the interaction between "A" and "A" segments on the self-assembly of the diblock dendrimer, $\epsilon^*_{AA} = 3$, 5, 8, and 10 are considered.

Figure 6 shows the average packing fraction of segments of the dendrimer in the slit of $H = 8\sigma$ as a function of bulk packing fraction at the different interactions of ϵ^*_{AA}. When $\epsilon^*_{AA} = 3$, the average packing fraction of the dendrimer in the slit increases linearly with the bulk packing fraction in the whole range studied. However, when $\epsilon^*_{AA} = 5$ and 8, both curves present an abrupt jump, and the two jumps are located at the bulk packing fraction $\eta_{bulk} = 0.1$ and 0.054, which suggests that the dendrimers in the slit have a strong trend for self-assembly. The abrupt jump corresponds to the first-order phase transition from a disordered state to an ordered phase, which has been discussed in previous publications for the flexible chains.[44]

To further get insight into the microscopic structure corresponding to the jump, parts a and b of Figure 7 show the local density profiles of "A" and "B" segments at $\epsilon^*_{AA} = 5$ before and after the jump, that is, at the bulk packing fraction of $\eta_{bulk} = 0.099$ and 0.1, respectively. Obviously, the density profiles at $\eta_{bulk} = 0.099$ present a disordered state of confined dendrimers without any phase separation in the slit, while the density profiles at $\eta_{bulk} = 0.1$ indicate that the phase separation of two blocks denoted by "A" and "B" appears distinctly. Furthermore, the confined dendrimers present a lamellar ordered structure of the BAB trilayer film, where the arm composed of "A" segments is orderly arranged in the center of the slit while the other two arms composed of "B" segments are arranged near the walls. Interestingly, the curve of $\epsilon^*_{AA} = 5$ in Figure 6 presents an abrupt drop at the bulk packing fraction $\eta_{bulk} = 0.234$. To explore the reason, we show in Figure 7c,d the microstructures of the dendrimers in the slit at $\eta_{bulk} = 0.234$ and $\eta_{bulk} = 0.235$. It is observed from Figure 7c,d that the trilayer film structure translates into a five-layer film as the bulking packing fraction increases from $\eta_{bulk} = 0.234$ to 0.235. Hence, the abrupt drop in the curve of $\epsilon^*_{AA} = 5$ at $\eta_{bulk} = 0.234$ is attributed to the morphological change of the film from trilayer to five-layer structures. Obviously, it is the increase of the bulk packing fraction that causes the morphological change in the film. The schematic diagrams corresponding to the trilayer and five-layer films are shown in Figure 8.

Figure 9 shows the local density profiles of "A" and "B" segments at the bulk packing fractions of $\eta_{bulk} = 0.054$ and 0.055 at $\epsilon^*_{AA} = 8$. The obtained results indicate that the dendrimers are in a disordered state at $\eta_{bulk} = 0.054$ and in an ordered state at $\eta_{bulk} = 0.055$. Compared to the microstructure of the dendrimers at $\epsilon^*_{AA} = 5$, the local densities at $\epsilon^*_{AA} = 8$ present more ordered layer structure, which is reflected in high peak value of local densities, especially in the center of the slit.

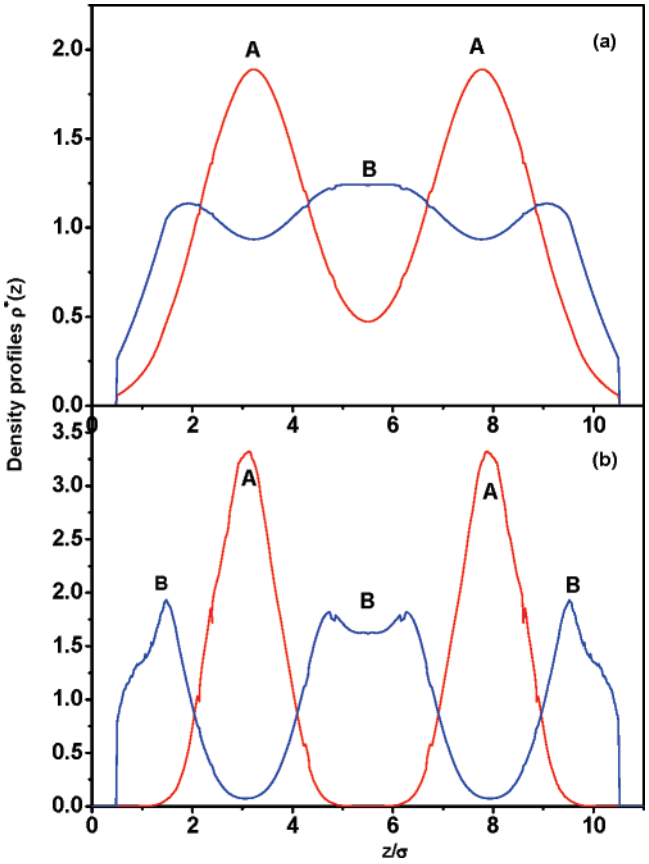

Figure 12. Microstructures of the dendrimers of G2 in the slit of $H = 11\sigma$ at $\epsilon^*_{AA} = 5$ and different bulk packing fractions: (a) $\eta_{bulk} = 0.097$; (b) $\eta_{bulk} = 0.098$.

Obviously, the critical bulk packing fraction, corresponding to the first-order phase transition from the disordered to ordered state, increases with the increase of ϵ^*_{AA} value from 5 to 8.

To explore the effect of the width of the slit on the self-assembly of the confined dendrimers, we consider behavior of the dedrimers in the slit of $H = 11\sigma$. Figure 10 shows the average packing fraction of segments of the dendrimers in the slit of $H = 11\sigma$ as a function of the bulk packing fraction at $\epsilon^*_{AA} = 3$, 5, 8, 10 and 12. When $\epsilon^*_{AA} = 3$, the average packing fraction of the dendrimers in the slit shows a slight jump at $\eta_{bulk} = 0.15$. Figure 11 shows the microstructures of the dendrimers before and after the jump, that is, at $\eta_{bulk} = 0.15$ and 0.17. The density profiles of the dendrimer at $\eta_{bulk} = 0.15$ only present a trend for the phase separation of two blocks with different properties. On the contrary, the dendrimer at $\eta_{bulk} = 0.17$ presents the complete phase separation of two blocks with different properties. In addition, it is observed that all the curves of $\epsilon^*_{AA} = 5$, 8, 10, and 12 in Figure 10 show the abrupt jump and the corresponding critical bulk packing fractions are located at $\eta_{bulk} = 0.097$, 0.038, 0.05, and 0.085. It suggests that in these cases the dendrimers are abruptly self-assembled into a lamellar thin film from the disordered state, which is the same as the behavior in the slit of $H = 8\sigma$. The microstructures shown in Figures 12 and 13 testify the above observation.

We can also observe from Figure 13b that the density profiles approximate zero in the range of a contact point to $z = 1.2\sigma$. Hence, the dendrimers self-assemble into a trilayer lamellar thin film in Figure 13b. However, the trilayer lamellar film is thinner than the slit. Accordingly, a vacuum space near the wall is formed. The vacuum space can provide as the adjuster for the thickness of the lamellar film. When the bulk packing fraction

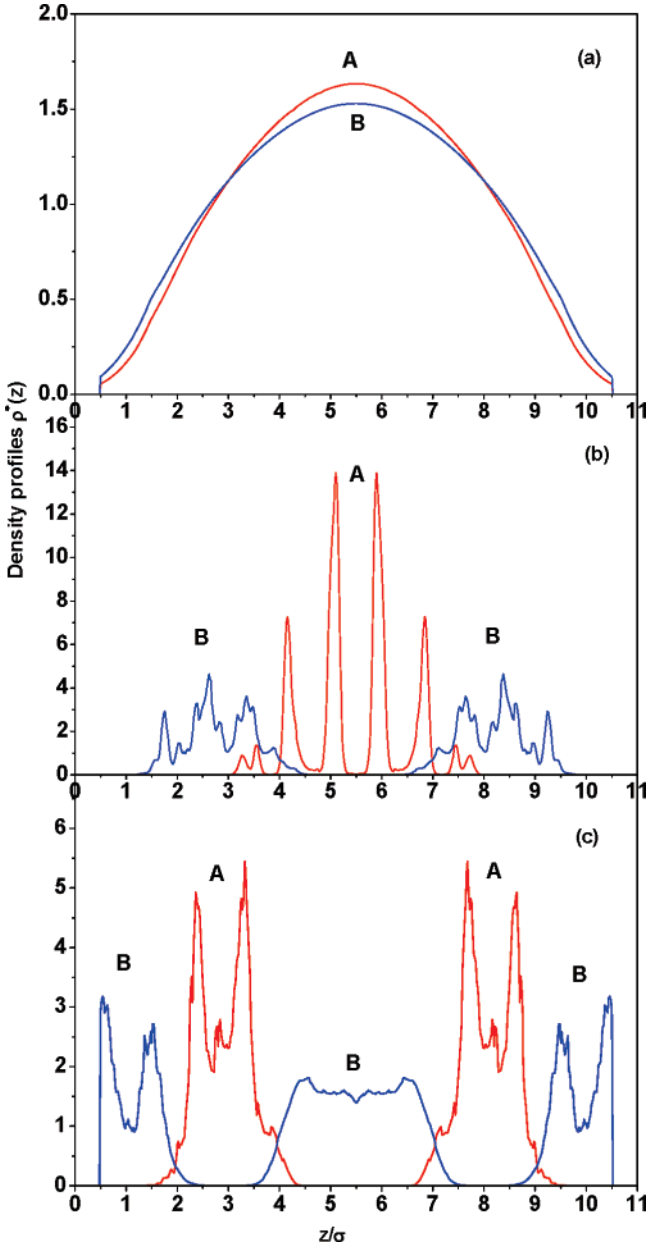

Figure 13. Microstructures of the dendrimers of G2 in the slit of $H = 11\sigma$ at $\epsilon^*_{AA} = 8$ and different bulk packing fractions: (a) $\eta_{bulk} = 0.038$; (b) $\eta_{bulk} = 0.039$; (c) $\eta_{bulk} = 0.09$.

increases to $\eta_{bulk} = 0.09$, the morphology of the dendrimer thin film changes to a five-layer lamellar film. The morphological change is due to the thickness change of the lamellar film. Compared to Figure 13b,c, it is found that the thickness of the five-layer lamellar film is smaller than that of the trilayer lamellar film. To illustrate the difference of the ordered structures in Figure 13b,c, the schematic diagrams of the trilayer and five-layer lamellar films are shown in Figure 14.

Interestingly, it can be observed from Figure 10 that when $\epsilon^*_{AA} = 3$, 5, 8, 10, and 12, the critical bulk packing fractions, corresponding to the first-order phase transition from disordered state to the self-assembly, are equal to 0.15, 0.097, 0.038, 0.05, and 0.085, respectively. Obviously, it is at $\epsilon^*_{AA} = 8$ rather than $\epsilon^*_{AA} = 10$ or 12 that the minimum critical bulk packing fraction appears; this observation is distinctively different from the case of self-assembly of the rod-like molecules in the slit, where the critical bulk concentration increases with the decrease of the head−head interaction linearly.[49] The reason may be that the

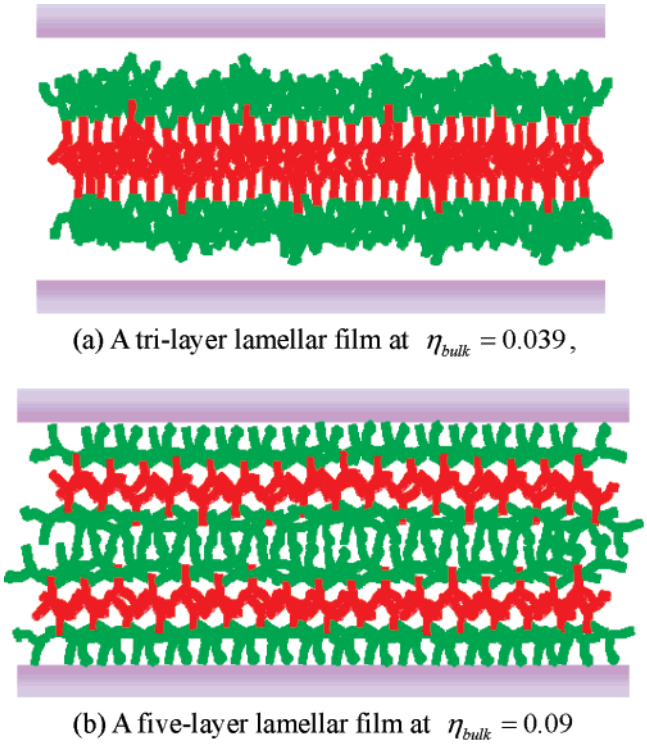

Figure 14. Schematic diagrams for the lamellar thin films formed by the self-assembly of dendrimers in the silt of $H = 11\sigma$ at $\epsilon^*_{AA} = 8$: (a) trilayer lamellar film at $\eta_{bulk} = 0.039$; (b) five-layer lamellar film at $\eta_{bulk} = 0.09$.

extremely strong interaction between "A" segments leads to the aggregation of the dendrimers in the bulk phase. The formation of the aggregation causes the difficulty for the dendrimer entering the confined space. Compared with these cases of $\epsilon^*_{AA} = 3$, 5, and 8 in the range of $\eta_{bulk} < 0.06$, the smaller average packing fraction of the dendrimer of $\epsilon^*_{AA} = 10$ in the slit confirms the above assumption. It is worth noting that when ϵ^*_{AA} increases from 10 to 12, the critical bulk concentration also increases from 0.05 to 0.085. This is due to the formation of the bigger aggregates, which leads to strong depletion effect blocking the dendrimer to enter the confinement.

It should be pointed out that the curves of the average packing fraction in the slit of $H = 11\sigma$ are much more sophisticated than those at $H = 8\sigma$, and the critical bulk density has a minimum at $\epsilon^*_{AA} = 8$. This may be because the distance of $H = 8\sigma$ is close in value to the thickness of the films formed by the dendrimer molecules naturally, while the distance of $H = 11\sigma$ is larger or smaller than the natural thickness.

4. Conclusion

In this work, a hybrid approach was used to investigate the microscopic properties of hard dendrimers and self-assembly of diblock dendrimers between two hard walls. The hybrid approach contains a single-chain Monte Carlo simulation for the calculation of the ideal-gas contribution of the Helmholtz energy and a DFT approach for the evaluation of the excess Helmholtz energy. The DFT approach includes a modified fundamental measure theory for the excluded-volume effect, the first-order thermodynamics perturbation theory for the chain connectivity, and mean-field approximation for the van der Waals attraction.

In the athermal system, we investigated the effects of generations and bulk packing fraction on the microstructures of hard dendrimers confined between two hard walls. With the increase of generations, the complexity of the dendritic architecture increases. Therefore, the depletion effect becomes stronger with the increase of the generation at $\eta_{bulk} = 0.1$. In addition, with the increase of the bulk packing fraction, the packing effect of the confined fluids would replace the depletion effect. It is also found that the structural complexity of the dendrimer leads to an increase in the critical bulk packing fraction corresponding to the transition from depletion effect to packing effect. Finally, we found that the more complex the molecular architecture and the higher the molecular stiffness, the smaller is the partitioning coefficient.

In the thermal system, we explored the effects of the width of the slit and the interaction (ϵ^*_{AA}) between segments "A" on the self-assembly of the diblock dendrimer. With the increase of ϵ^*_{AA}, we observed the abrupt jump in the curves of the average packing fraction of the dendrimers in both slits of $H = 8\sigma$ and 11σ. The abrupt jump corresponds to the first-order phase transition from a disordered state to a lamellar ordered structure. Interestingly, in the slit of $H = 11\sigma$, it is at $\epsilon^*_{AA} = 8$ rather than $\epsilon^*_{AA} = 10$ or 12 that the minimum critical bulk packing fraction appears. This observation is distinctively different from the case of self-assembly of the rod-like molecules in the slit, where the critical bulk concentration increases with the decrease of the head−head interaction linearly. In addition, in the two cases of $H = 11\sigma$, $\epsilon^*_{AA} = 8$ and $H = 8\sigma$, $\epsilon^*_{AA} = 5$, we observed a morphological change of the lamellar films from the trilayer to five-layer microdomains with the increase of the bulk packing fraction. It is worth noting that although a lot of molecular simulations have been performed to predict the thermodynamic properties of the dendrimers, this is the first report applying the DFT to investigate the properties of the dendrimers. It is expected that further DFT calculations would contribute to the properties of the dendrimers.

Acknowledgment. This work is supported by National Natural Science Foundation of China (No. 20646001), Beijing Novel Program (No. 2006B17), The Program for New Century Excellent Talents in University (NCET-06-0095), and the "Chemical Grid Program" and Excellent Talents Funding of Beijing University of Chemical Technology.

References and Notes

(1) Tomalia, D. A.; Frechet, J. M. J. *J. Polym. Sci., Part A: Polym. Chem.* **2002**, *40*, 2719.
(2) Tomalia, D. A. *Macromol. Symp.* **1996**, *101*, 243.
(3) Naj, A. K. *Wall St. J.* **1996**, *B1*.
(4) Tomalia, D. A. *Prog. Polym. Sci.* **2005**, *30*, 294.
(5) Frechet J. M. J.; Tomalia. D. A. *Dendrimers and Other Dendritic Polymers*; Wiley: Chichester, U.K., 2001.
(6) Tomalia, D. A.; Baker, H.; Dewald, J.; Hall, M.; Kallos, G.; Martin, S. e. a. *Polym. J.* **1985**, *17*, 117.
(7) Buhleier, G. E.; Wehner, W.; Vogtle, F. *Synthesis* **1978**, 155.
(8) Ballauff, M.; Likos, C. N. *Angew. Chem., Int. Ed.* **2004**, *43*, 2998.
(9) Lee, I.; Athey, B. D.; Wetzel, A. W.; Meixner, W.; Baker, J. R. *Macromolecules* **2002**, *35*, 4510.
(10) Darbre, T.; Reymond, J.-L. *Acc. Chem. Res.* **2006**.
(11) Dhanikula, R. S.; Hildgen, P. *Bioconjugate Chem.* **2006**, *17*, 29.
(12) Lim, J.; Simanek, E. E. *Mol. Pharmacol.* **2005**, *2*, 273.
(13) Ooe, M.; Murata, M.; Mizugaki, T.; Ebitani, K.; Kaneda, K. *J. Am. Chem. Soc.* **2004**, *126*, 1604.
(14) Hoover, N. N.; Auten, B. J.; Chandler, B. D. *J. Phys. Chem. B* **2006**, *110*, 8606.
(15) Lafaye, G.; Siani, A.; Marecot, P.; Amiridis, M. D.; Williams, C. T. *J. Phys. Chem. B* **2006**, *110*, 7725.
(16) Bar-Haim, A.; Klafter, J. *J. Phys. Chem. B* **1998**, *102*, 1662.
(17) Wang, S.; Wang, X.; Li, L.; Advincula, R. C. *J. Org. Chem.* **2004**, *69*, 9073.
(18) Kaanumalle, L. S.; Ramesh, R.; MurthyMaddipatla, V. S. N.; Nithyanandhan, J.; Jayaraman, N.; Ramamurthy, V. *J. Org. Chem.* **2005**, *70*, 5062.

(19) Ong, W.; Kaifer, A. E. *J. Am. Chem. Soc.* **2002**, *124*, 9358.
(20) Boubbou, K. H.; Ghaddar, T. H. *Langmuir* **2005**, *21*, 8844.
(21) Kovvali, A. S.; Sirkar, K. K. *Ind. Eng. Chem. Res.* **2001**, *40*, 2502.
(22) Xiao, Y.; Chung, T.-S.; Chng, M. L. *Langmuir* **2004**, *20*, 8230.
(23) Li, W. S.; Kim, K. S.; Jiang, D. L.; Tanaka, H.; Kawai, T.; Kwon, J. H.; Kim, D.; Aida, T. *J. Am. Chem. Soc.* **2006**, *128*, 10527.
(24) Han, M.; Chen, P. Q.; Yang, X. Z. *Polymer* **2005**, *46*, 3481.
(25) Suek, N. W.; Lamm, M. H. *Macromolecules* **2006**, *39*, 4247.
(26) Lee, H.; Baker, J. R.; Larson, R. G. *J. Phys. Chem. B* **2006**, *110*, 4014.
(27) Mansfield, M. L. *Polymer* **1996**, *37*, 3835.
(28) Gorman, C. B.; Smith, J. C. *Polymer* **2000**, *41*, 675.
(29) Welch, P. M. *Nano Lett.* **2005**, *5*, 1279.
(30) Zhou, T.; Chen, S. B. *Macromolecules* **2005**, *38*, 8554.
(31) Rissanou, A. N.; Economou, I. G.; Panagiotopoulos, A. Z. *Macromolecules* **2006**, *39*, 6298.
(32) Ni, R.; Cao, D. P.; Wang, W. C. *J. Phys. Chem. B* **2006**, *110*, 26232.
(33) Chandler, D.; McCoy, J. D.; Singer, S. J. *J. Chem. Phys.* **1986**, *85*, 5971.
(34) McCoy, J. D.; Ye, Y.; Curro, J. G. *J. Chem. Phys.* **2003**, *117*, 2975.
(35) Woodward, C. E. *J. Chem. Phys.* **1991**, *94*, 3183.
(36) Nath, S. K.; Nealey, P. F.; de Pablo, J. J. *J. Chem. Phys.* **1999**, *110*, 7483.
(37) Kierlik, E.; Rosinberg, M. L. *J. Chem. Phys.* **1992**, *97*, 9222.
(38) Yu, Y. X.; Wu, J. Z. *J. Chem. Phys.* **2002**, *117*, 10156.
(39) Roth, R.; Evans, R.; Lang, A.; Kahl, G. *J. Phys.: Condens. Matter* **2002**, *14*, 12063.
(40) Tripathi, S.; Chapman, W. G. *Phys. Rev. Lett.* **2005**, *94*, 087801.
(41) Ye, Z. C.; Cai, J.; Liu, H. L.; Hu, Y. *J. Chem. Phys.* **2005**, *123*, 194902.
(42) Cao, D. P.; Wu, J. Z. *Macromolecules* **2005**, *38*, 971.
(43) Li, Z. D.; Cao, D. P.; Wu, J. Z. *J. Chem. Phys.* **2005**, *122*, 174708.
(44) Bryk, P.; Sokolowski, S. *J. Chem. Phys.* **2004**, *120*, 8299.
(45) Fu, D. *J. Chem. Phys.* **2006**, *124*, 164701.
(46) Cao, D. P.; Wu, J. Z. *Langmuir* **2005**, *21*, 9786.
(47) Kim, S. C.; Lee, S. H. *J. Chem. Phys.* **2006**, *125*, 046101.
(48) Cao, D. P.; Wu, J. Z. *J. Chem. Phys.* **2004**, *121*, 4210.
(49) Cao, D. P.; Zhu, M. H.; Wang, W. C. *J. Phys. Chem. B* **2006**, *110*, 21882.
(50) Cao, D. P.; Jiang, T.; Wu, J. Z. *J. Chem. Phys.* **2006**, *124*, 164904.
(51) Malijevsky, A.; Bryk, P.; Sokolowski, S. *Phys. Rev. E* **2005**, *72*, 032801.
(52) Li, Z. D.; Cao, D. P.; Wu, J. Z. *J. Chem. Phys.* **2005**, *122*, 224701.
(53) Cao, D. P.; Wu, J. Z. *J. Chem. Phys.* **2005**, *122*, 194703.
(54) Zhang, X. R.; Cao, D. P.; Chen, J. F. *J. Phys. Chem. B* **2003**, *107*, 4942.
(55) Bryk, P.; Bucior, K.; Sokolowski, S.; Zukocinski, G. *J. Phys. Chem. B* **2005**, *109*, 2977.
(56) Bryk, P.; Pizio, O.; Sokolowski, S. *J. Chem. Phys.* **2005**, *122*, 194904.
(57) Cao, D. P.; Wu, J. Z. *Langmuir* **2006**, *22*, 2712.
(58) Karatasos, K. *Macromolecules* **2006**, *39*, 4619.
(59) Rosenfeld, Y. *Phys. Rev. Lett.* **1989**, *63*, 980.
(60) Yethiraj, A.; Woodward, C. E. *J. Chem. Phys.* **1995**, *102*, 5499.
(61) Sen, S.; Cohen, J. M.; McCoy, J. D.; Curro, J. G. *J. Chem. Phys.* **1994**, *101*, 9010.